Frontiers in Bioscience Landmark

Front. Biosci. (Landmark Ed) **2025**; 30(3): 27082
https://doi.org/10.31083/FBL27082

Original Research

Dapagliflozin Attenuates Myocardial Inflammation and Apoptosis after Coronary Microembolization in Rats by Regulating the SIRT1/NF-κB Signaling Pathway

Tao Li[1,†], Chang-Jun Luo[1,2,†], Ze-Qiang Yi[1], Lang Li[1,*]

[1]Department of Cardiology, The First Affiliated Hospital of Guangxi Medical University, 530021 Nanning, Guangxi, China
[2]Department of Cardiology, Affiliated Liutie Central Hospital of Guangxi Medical University, 545007 Liuzhou, Guangxi, China
*Correspondence: drlilang@gxmu.edu.cn (Lang Li)
[†]These authors contributed equally.

Academic Editor: Rajesh Katare
Submitted: 22 October 2024 Revised: 30 November 2024 Accepted: 9 December 2024 Published: 18 March 2025

Abstract

Background: Coronary microembolization (CME) often occurs as a serious complication during or after percutaneous coronary intervention (PCI), leading to an impairment in heart function, inflammation, and cell death. Dapagliflozin (DAPA) has been shown to have cardioprotective effects. However, its role and exact mechanism in CME remains unclear. **Methods**: A preclinical CME model was developed via the administration of microspheres into the left ventricle. In an in vitro model, the CME-created microenvironment was observed by using lipopolysaccharide (LPS) with hypoxic induction on H9C2 cardiomyocytes. Before developing both experimental models, DAPA or the sirtuin 1 (SIRT1) inhibitor "EX-527" was administered. Echocardiography, histological examination, and molecular and immunological assays were carried out to assess the levels of cardiac tissue or cardiomyocyte damage, inflammation, and apoptosis. **Results**: Heart dysfunction and tissue damage caused by CME can be alleviated by pre-treatment with DAPA, which also reduces myocardial inflammation and apoptosis. Moreover, both experimental studies have depicted that DAPA can upregulate the SIRT1 level and downregulate the acetylation and phosphorylation levels of nuclear factor kappa-B (NF-κB) p65. This effect inhibits the induction of NF-κB signaling and mitigates cardiomyocyte damage. However, DAPA's cardioprotective effect was reversed when co-treated with EX-527. **Conclusions**: DAPA reduces myocardial damage caused by CME by suppressing myocarditis and apoptosis via the SIRT1/NF-κB axis.

Keywords: dapagliflozin; apoptosis; inflammation; SIRT1; coronary microembolization

1. Introduction

Coronary microembolization (CME), which frequently results from percutaneous coronary intervention (PCI) or thrombolytic treatment, is typically due to the disruption of weak atherosclerotic plaques or obstruction of the distal end of the coronary artery by plaque debris or small thrombi [1–3]. During peri-operation, the typical occurrence rate of CME is 15–20%, increasing to as high as 45% in high-risk patients [4,5]. Local heart contractile impairment and fatal arrhythmias can be the result of CME causing slow flow or no flow in the heart tissue. This adversely affects patient cardiac functions and diagnosis [6,7]. It has been found that a high number of necrotic or apoptotic cardiomyocytes and substantial inflammatory cell infiltration linked to with CME-induced myocardial micro-infarctions. This mechanism is responsible for CME-induced myocardial injury and heart dysfunction. Thus, targeting myocarditis and apoptosis can be considerably improved, thereby reducing myocardial injury and improving cardiac function [8,9]. Anti-inflammatory, antithrombotic agents, and vasodilators are the main treatments used for the prevention of CME [3]. Thus, it is necessary to establish effective strategies for the prevention and management of CME.

Sirtuin 1 (SIRT1), a member of the sirtuin family, is a highly conserved NAD^+-dependent deacetylase that functions as a post-translational regulator [10]. Its deacetylation activity plays a crucial role in various biological processes, including oxidative stress (OS), cellular senescence, inflammation, and apoptosis [11–13]. SIRT1 has been found to suppress the nuclear factor kappa-B (NF-κB) axis, thus reducing inflammation in myocardial-infarcted rats [14]. A recent study found that right ventricular pacing led to increased fibrosis and a suppression of SIRT1 in the left atrium of pigs, whereas biventricular pacing upregulated its expression [15]. A previous study demonstrated that resveratrol reduces cardiomyocyte apoptosis in rats that have been exposed to CME by deacetylating p53 through the SIRT1 pathway [16]. Thus, regulation of SIRT1 levels offers a potential therapeutic strategy targeting cardiovascular diseases (CVDs).

Dapagliflozin (DAPA) is an oral hypoglycemic drug that is a member of a novel class of drugs identified as sodium-glucose cotransporter 2 (SGLT2) inhibitors. It acts by blocking glucose reabsorption in the kidneys and enhancing its excretion in urine [17,18]. Apart from its glucose-reducing abilities, DAPA has a substantial role in CVDs [19]. Clinical studies have shown that DAPA

markedly decreases the possibility of cardiovascular mortality and is required for hospitalized heart failure patients [20,21]. A study has suggested that DAPA can reduce inflammation and apoptosis in hyperglycemic endothelial cells by stimulating adenosine monophosphate-activated protein kinase (AMPK)/SIRT1 pathway [22]. It was also shown that DAPA inhibits endoplasmic reticulum stress and activates SIRT1 to reduce pressure overload-induced myocardial remodeling in laboratory animals [23]. However, the function and possible mechanism of DAPA in heart injury caused by CME remain unclear.

Thus, the present research endeavors to elucidate the impact of DAPA on CME-induced myocarditis and apoptosis in rats, and to investigate its connection with SIRT1 and downstream pathways. This, in turn, will reveal the potential mechanism and role of DAPA in the context of heart damage caused by CME.

2. Materials and Methods

2.1 Animal Model

Eight-week-old male Sprague-Dawley (SD) rats (Guangxi Medical University, Nanning, Guangxi, China), weighing between 250 and 300 grams, were acquired and housed at the Guangxi Medical University's Experimental Animal Facility. All animal-related experiments, conducted in accordance with the established standards and procedures of the National Institutes of Health, have been approved by the Animal Care and Welfare Committee of Guangxi Medical University.

The CME rat model was established as previously described [8]. The rats were intraperitoneally administered with 1% pentobarbital sodium (30–40 mg/kg) to induce anesthesia. After completing tracheal intubation and assisting rat respiration with an animal ventilator, the chest was opened to expose the heart, and the ascending aorta was exposed and occluded for 10 sec with a vascular clamp, and 4000 microspheres (45 µm) (Polysciences Inc., Warrington, PA, USA) in normal saline (0.2 mL) were infused into the left ventricle from the apex of the heart. The sham group was only treated with 0.2 mL of normal saline and followed by the same surgical and experimental procedures. The chest was closed sequentially, and extubation was performed when heart rate and spontaneous respiration were restored.

2.2 Experimental Groups

All experimental rats were distributed into 4 groups randomly: (1) Sham, (2) CME, (3) CME + DAPA, and (4) CME + DAPA + EX-527 groups. Each group consisted of 10 rats (n = 10). Before the establishment of the CME model, rats in the CME + DAPA group received pretreatment of DAPA (1 mg/kg/d) (AstraZeneca Pharmaceutical Co., Ltd., Cambridge, UK) through intragastric injection for 7 days. The dose setting was based on studies of other metabolic and CVD models, along with the equal volume of drug doses between rat and human body surface area [24–26]. Dapagliflozin was administered to rats in the CME+ DAPA + EX-527 group for 7 days, followed by EX-527 (5 mg/kg) (MedChem Express Co., Nanjing, Jiangsu, China) in the tail vein for 30 min before surgery. We previously found that the heart's functionality was at its lowest point 12 h after the CME [8]. Echocardiography was conducted 12 h after CME induction. Following this, the experimental rats were euthanized by intraperitoneal injection of an overdose of 1% pentobarbital sodium, and blood and cardiac tissues were collected.

2.3 Echocardiography

To evaluate cardiac function in rats postoperatively, the left ventricular end-diastolic diameter (LVEDd), left ventricular fractional shortening (LVFS), left ventricular end-systolic diameter (LVESd), and left ventricular ejection fraction (LVEF) were measured by an ultrasonic cardiograph (Philips Technologies, Andover, MA, USA). All echocardiograms were carried out by trained specialists who were unaware of the study.

2.4 Hematoxylin and Eosin (HE) Staining

The rat ventricle's 4 µm paraffin sections underwent deparaffinization and rehydration processes, followed by staining with hematoxylin and eosin. These sections were dehydrated and dried. All histological key features were observed and analyzed under optical microscopy (Olympus, Tokyo, Japan).

2.5 Transmission Electron Microscopy (TEM)

The myocardium's ultrastructural features were examined through the application of TEM. The myocardium of the left ventricular free wall was divided into 1 mm^3 sections, immersed in 3% glutaraldehyde for 24 h at 4 °C, and then dehydrated, embedded, and stained with respective stainings. Utilizing the Hitachi H-7650 electron microscope (Hitachi, Tokyo, Japan), these sections underwent a thorough examination.

2.6 Detection of Cardiomyocyte Injury Markers

Cell culture supernatants or serum samples were evaluated for the detection of the level of creatine kinase myocardial band isoenzyme (CK-MB), cardiac troponin I (cTnI), interleukin-1β (IL-1β) and tumor necrosis factor-α (TNF-α) via commercial ELISA kits (Bio-Swamp, Wuhan, Hubei, China). Lactate dehydrogenase (LDH) activity was quantified using a kit (Solarbio, Beijing, China). Superoxide dismutase (SOD) activity, malondialdehyde (MDA) content and adenosine triphosphate (ATP) levels were evaluated with respective SOD, MDA, and ATP measurement kit (Beyotime, Shanghai, China), as per the manufacturers' recommendations.

2.7 Hematoxylin-Basic Fuchsin-Picric Acid (HBFP) Staining

Myocardial micro-infarction in rats after CME induction was evaluated using HBFP staining. About 4 µm ventricular heart paraffin sections were deparaffinized, stained with hematoxylin, and alkaline fuchsin, and differentiated in a picric acid acetone dye. These sections were dried and dehydrated. These results were evaluated with an optical microscope (Olympus, Tokyo, Japan). All erythrocytes and ischemic myocardial tissues were stained red, while the nuclei were stained blue-black, and the normal myocardial tissues were stained yellow or brownish-yellow. The infarct size was quantified via Image J software (NIH, Bethesda, MD, USA).

2.8 Immunohistochemical Staining

Precisely, the tissue sections were processed for deparaffinization, hydration, and antigen retrieval steps. The sections were kept with primary antibodies: IL-1β (1:500, ab283818, Abcam, Cambridge, UK) and TNF-α (1:500, ab307164, Abcam, Cambridge, UK) with 1:500 dilutions and then labeled with HRP polymer-linked secondary antibody (1:1000, ab6721, Abcam, Cambridge, UK). The results were examined under the optical microscope.

2.9 Cell Culture and Group Distribution

Rats H9C2 cardiomyocytes (Zhongqiao Xinzhou Biotechnology Co., Ltd., Shanghai, China) were used for *in vitro* model induction. A complete cell culture medium was prepared by supplementing 10% fetal bovine serum (FBS; Gibco, Waltham, MA, USA) with Dulbecco's Modified Eagle Medium (DMEM; Gibco, MA, USA). The cell culture was maintained at 37 °C in a 5% CO_2. The H9C2 cell line has passed short tandem repeat (STR) profiling validation and tested negative for mycoplasma. In the previous study, a cell model was developed by exposing the cells from lipopolysaccharide (LPS) (Solarbio, Beijing, China) along with hypoxia to create an ischemia microenvironment caused by CME and induced cardiac damage [27]. H9C2 was treated with LPS (10 µg/mL) under hypoxic conditions for 12 h to induce injury. Control cells were cultured under a controlled environment without any treatment. Before exposing the cells to LPS + hypoxia stimulation, they were pre-treated with 10 µM dapagliflozin for 2 h for DAPA treatment. In the rescue experiment, cells were pre-treated with DAPA and EX-527 (10 µM) for 2 h before being induced with LPS+ hypoxia (LPS+H).

2.10 Cell Viability

In all groups, approximately 5×10^3/well H9C2 cells were allowed to grow into a 96-well plate. After addition of CCK-8 solution (10 µL, Solarbio, Beijing, China) for 1 h at 37 °C, absorbances at 450 nm were read with a microplate reader (Thermo Inc., Waltham, MA, USA).

2.11 Measurement of ROS Generation

Each group of samples was treated with a sensitive fluorogenic probe called dihydroethidium (DHE) to assess the reactive oxygen species (ROS) accumulation within the cells. Both H9C2 cells and frozen heart tissue sections were treated with 10 mM of DHE (Servicebio, Guangzhou, Guangdong, China) for 30 min at 37 °C in dark conditions. After incubation, the fluorescence emitted by the tissues and cells was recorded using a fluorescent microscope (Olympus, Tokyo, Japan). The ROS signals were measured via the ImageJ software (1.51j, National Institute of Health, Bethesda, MD, USA).

2.12 TdT-Mediated dUTP Nick-End Labeling (TUNEL) Staining

Apoptosis rates in H9C2 cardiomyocytes and heart tissue sections were assessed with a TUNEL Cell Apoptosis Detection Kit (Servicebio, Guangzhou, China). Briefly, the sections were incubated with the TUNEL reaction reagent to stain apoptotic cells, with 4',6-diamidino-2-phenylindole (DAPI, Solarbio, Guangzhou, Guangdong, China) counterstaining of the nuclei to assess the number of cells. These sections were then examined under a fluorescence microscope (Olympus, Tokyo, Japan). The proportion of apoptotic cardiomyocytes was measured by dividing the number of TUNEL+ve cardiomyocyte nuclei by the overall number of cardiomyocyte nuclei.

2.13 Immunofluorescence (IF) Staining

IF was employed to assess levels of apoptosis-associated proteins in H9C2 cardiomyocytes and rat heart tissues. Briefly, cardiomyocyte slides and heart tissue sections were immersed in paraformaldehyde (PFA, 4%), permeabilized with Triton-X (0.5%), and blocked with bovine serum albumin (5%). Sections were then treated with primary antibodies against SIRT1 (1:100, ab189494, Abcam, Cambridge, UK), Bcl-2 (1:300, ab194583, Abcam, Cambridge, UK), Bax (1:300, ab53154, Abcam, Cambridge, UK), and cleaved caspase-3 (1:300, #9661, Cell Signaling Technology, CST, Danvers, MA, USA) at 4 °C for 24 h. Subsequently, the sections were probed with Cy3-linked secondary antibodies (1:500, ab6939, Abcam, Cambridge, UK) in the dark for 1 h. DAPI (Solarbio, Guangzhou, Guangdong, China) was used to counterstain the cell nuclei. After each treatment step, the sections and slides are examined using a fluorescence microscope.

2.14 Western Blot (WB)

Proteins were isolated from rat heart tissues and H9C2 cells via radio immunoprecipitation assay (RIPA) buffer. After electrophoresis separation and transfer, the extracted proteins are transferred to the membrane, followed by blocking and primary antibody incubation. Primary antibodies included SIRT1 (1:1000, ab189494, Abcam, Cambridge, UK), TNF-α (1:1000, ab307164, Abcam, Cambridge, UK), Bax (1:1000, ab53154, Abcam,

Cambridge, UK), IL-1β (1:1000, ab283818, Abcam, Cambridge, UK), Bcl-2 (1:1000, ab194583, Abcam, Cambridge, UK), NF-κB P65 (1:1000, #8242, CST, Danvers, MA, USA), cleaved caspase-3 (1:1000, #9661, CST, Danvers, MA, USA), Phospho-NF-κB p65 (Ser536) (1:1000, #3033, CST, Danvers, MA, USA), and Acetyl-NF-κB p65 (Lys310) (1:1000, #3045, CST, Danvers, MA, USA). β-actin (1:10,000, ab8227, Abcam, Cambridge, UK) served as a reference internal control. Subsequently, the membrane is washed and incubated with the secondary antibody (1:10,000, sc-2357, Santa Cruz Biotechnology, Dallas, TX, USA). For protein band visualization, a chemiluminescence detection kit (Pierce, Rockford, IL, USA) was utilized. All bands were quantified via ImageJ software.

2.15 Statistical Analysis

Data was statistically evaluated via SPSS software (26.0 V, IBM, Chicago, IL, USA). All observations and analyses are represented as mean $\pm$ standard deviation (SD). Multiple group comparison was carried out via One-way analysis of variance (ANOVA) with Student-Newman-Keuls post hoc tests. A significance level of $p < 0.05$ was regarded as a significance threshold.

3. Results

3.1 DAPA Attenuates Cardiac Dysfunction and Myocardial Injury Induced by CME

The echocardiogram results indicated that heart function in the CME rats was substantially impaired as opposed to the Sham group. This was apparent in the higher LVEDd and LVESd, together with the reduced LVFS and LVEF. Conversely, the CME+DAPA group demonstrated improved LVFS and LVEF, together with decreased LVEDd and LVESd, relative to the CME rats, indicating that DAPA treatment greatly enhanced heart failure. The cardioprotective effect of DAPA can be reversed by EX-527 (Fig. 1A–E).

Myocardial tissues were histopathologically examined by HE and HBFP stainings. The HE-stained tissue section of the sham group did not show any apparent pathological abnormalities. However, the CME group revealed microembolic spheres within the arterioles, surrounded by areas of microinfarction. These areas were characterized by cell swelling, degeneration, erythrocyte extravasation, and invasion of inflammatory cells (Fig. 1F). The region of myocardial microinfarction is often detected using HBFP staining. The staining results indicated that the myocardium of rats in the sham group failed to show any apparent microinfarction, whereas the CME group displayed multiple microinfarctions (Fig. 1G,H). The CME group displayed higher levels of CK-MB, LDH, and cTnI relative to the Sham group, as per serum biochemical assays (Fig. 1I–K). After CME, these findings suggest severe cardiac damage and myocardial morphological abnormalities. Importantly, the pathological injury to myocardial tissue was ameliorated by DAPA pretreatment, which also resulted in a decrease in the severity of myocardial microinfarcts and the levels of serum CK-MB, LDH, and cTnI. Conversely, the positive effects of DAPA turned ineffective when combined with EX-527.

3.2 DAPA can Attenuate CME-Induced Mitochondrial Damage and Oxidative Stress

The TEM analysis of myocardial tissue revealed no abnormalities in the ultrastructure of the sham group. it was depicted that, the myocardial cell myofibrils were well-organized, and the mitochondrial membranes were intact. In contrast, the CME group displayed disorganized and partially fragmented myofibrils in myocardial cells. Vacuolar degeneration and swelling of mitochondria were also observed in the CME group. Moreover, the ultrastructural alterations and mitochondrial damage that were caused by CME were substantially alleviated by DAPA treatment (Fig. 2A). The myocardial cells in the CME group contained greater amounts of ROS and MDA, together with reduced SOD and ATP, relative to the Sham group. However, DAPA mitigated ROS production, increased ATP levels and SOD activity, and decreased MDA levels (Fig. 2B–F). Conversely, the antioxidant and mitochondrial therapeutic effects of DAPA were markedly reduced by co-treatment with EX-527. Collectively, these data indicate that DAPA reduces OS and mitochondrial injury induced by CME.

3.3 DAPA Attenuates H9C2 Cardiomyocyte Injury Induced by LPS Combined with Hypoxia

Relative to the controls, the viability of H9C2 cardiomyocytes in the LPS+H group decreased substantially, as indicated by the results of CCK-8 assays. Conversely, the viability of the cells was significantly enhanced by DAPA (Fig. 3A). The biochemical detection of CK-MB, LDH, and cTnI in the culture supernatant of the LPS+H group was higher than that of the controls. Following DAPA treatment, the levels of CK-MB, LDH, and cTnI in the supernatants decreased (Fig. 3B–D). Moreover, the LPS+H group of H9C2 cells exhibited greater ROS generation relative to the controls. Conversely, the formation of ROS decreased after DAPA treatment (Fig. 3E,F). However, the protective effect of DAPA on H9C2 cells was almost reversed by co-treatment with EX-527.

3.4 DAPA Attenuates CME-Induced Myocardial Inflammatory Damage

Serum levels of IL-1β and TNF-α were measured using ELISAs. In contrast to the sham group, the CME group revealed substantially elevated IL-1β and TNF-α levels in serum. However, their levels decreased after pretreatment with DAPA (Fig. 4A,B). The results of immunohistochemistry and WB indicated that the protein levels of IL-1β and TNF-α in the heart tissue of the CME group were substantially higher than those in the sham group, thereby confirming the presence of myocarditis after CME (Fig. 4C–E). However, their levels in rat myocardium de-

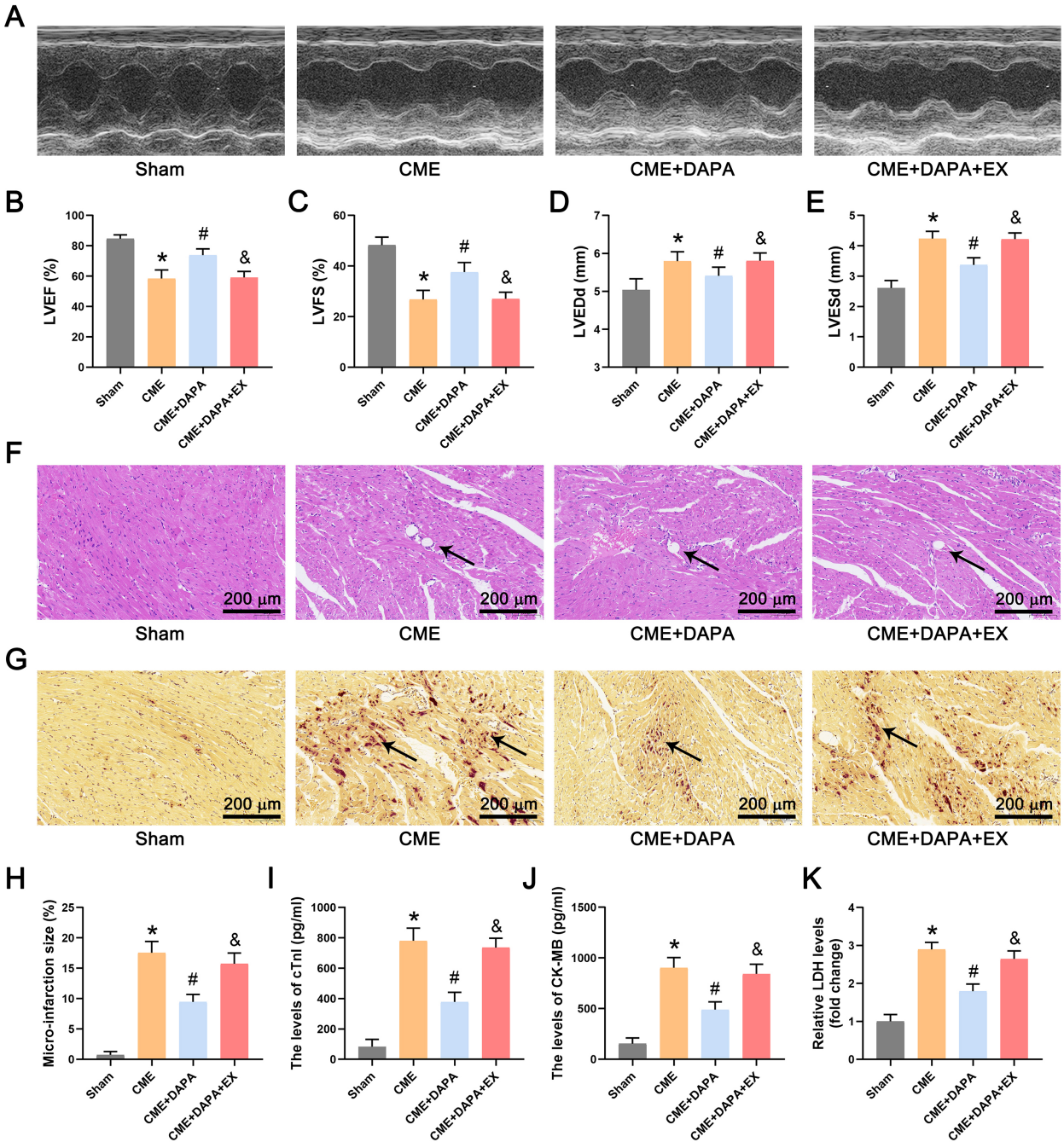

Fig. 1. DAPA attenuates cardiac dysfunction and myocardial injury induced by CME. (A) Images from echocardiography, representative of each group, are presented. (B–E) Measurement results of LVEDd, LVESd, LVEF, and LVFS (n = 10). (F) Representative images of HE-stained tissues each group (×200; scale bar = 200 μm). Black arrows indicate microspheres. (G) Images showing HBFP staining for each group (×200; scale bar = 200 μm). Black arrows indicate the microinfarct area. (H) Quantitative of the microinfarct areas in each group (n = 10). (I–K) Levels of cTnI, CK-MB, and LDH in serum measured for each group (n = 10). $*p < 0.05$ vs. the Sham group; $^{\#}p < 0.05$ vs. the CME group; $^{\&}p < 0.05$ vs. the CME + DAPA group. Abbreviations: CME, coronary microembolization; DAPA, dapagliflozin; EX, EX-527; LVEDd, left ventricular end-diastolic diameter; LVESd, left ventricular end-systolic diameter; LVEF, left ventricular ejection fraction; LVFS, left ventricular fractional shortening; HBFP, hematoxylin-basic fuchsin-picric acid; cTnI, cardiac troponin I; CK-MB, creatine kinase myocardial band isoenzyme; LDH, lactate dehydrogenase.

clined markedly after DAPA pre-treatment. Interestingly, the impact of DAPA on IL-1β and TNF-α levels decreased after co-treatment with EX-527.

3.5 DAPA Attenuates Cardiomyocyte Apoptosis Induced by CME

The apoptosis of cardiomyocytes was further assessed using TUNEL staining. In comparison to the sham group,

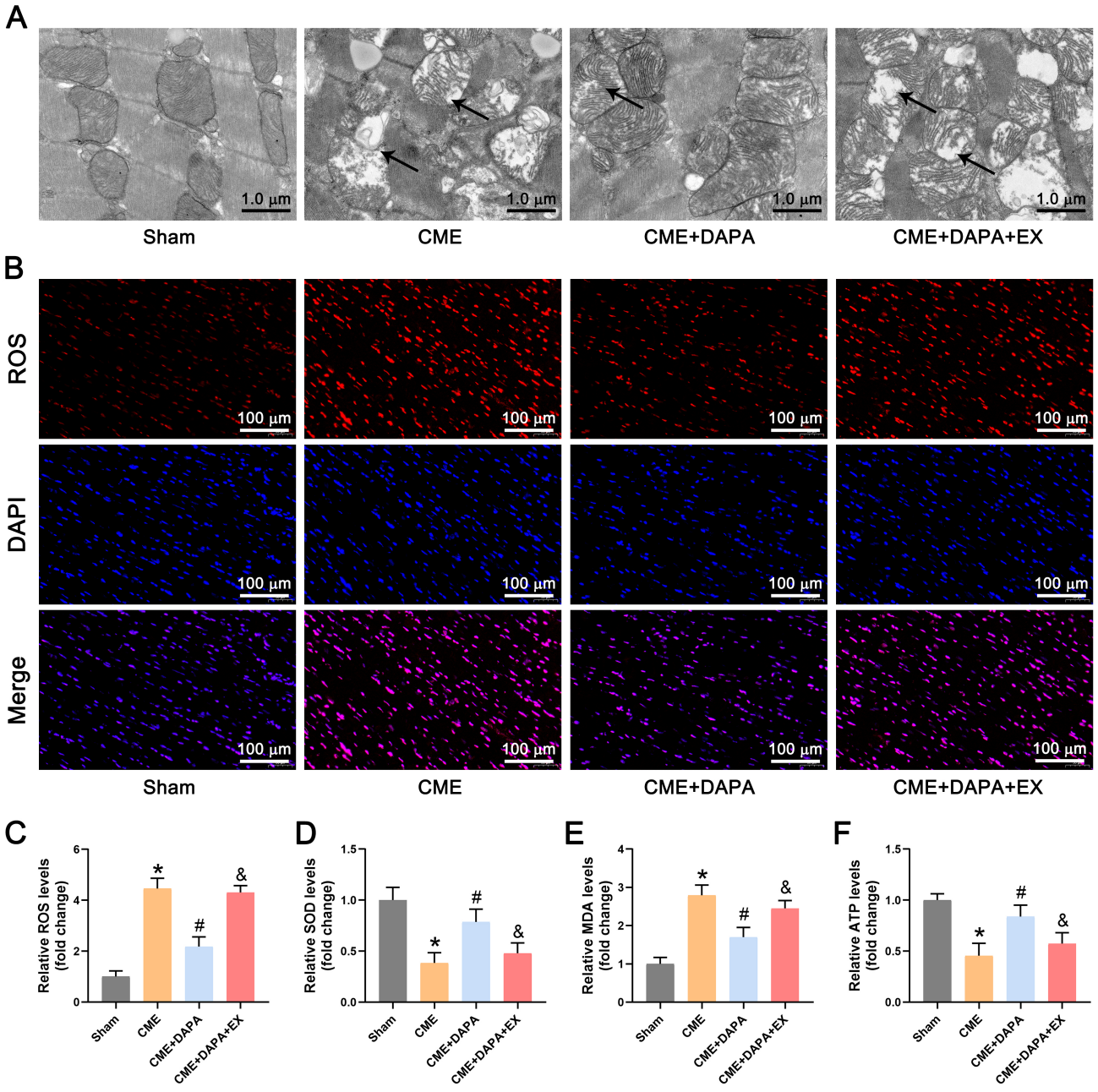

Fig. 2. DAPA can attenuate CME-induced mitochondrial damage and oxidative stress. (A) Representative TEM images from each group (×6000; scale bar = 1 μm). (B,C) DHE fluorescence probe was used to measure ROS production (×200; scale bar = 100 μm) (n = 10). (D–F) Assessment of MDA, SOD, and ATP levels in the different groups (n = 10). $^{*}p < 0.05$ vs. the Sham group; $^{\#}p < 0.05$ vs. the CME group; $^{\&}p < 0.05$ vs. the CME + DAPA group. Abbreviations: TEM, transmission electron microscopy; ROS, reactive oxygen species; MDA, malondialdehyde; SOD, superoxide dismutase; DHE, dihydroethidium.

the staining revealed a substantial increase number of TUNEL-positive nuclei in the CME group. DAPA pre-treatment led to a substantial reduction in the proportion of TUNEL-positive cardiomyocytes (Fig. 5A). The levels of apoptosis-related protein expression were analyzed using immunofluorescence staining and WB. In contrast to the sham group, the CME group showed substantially increased levels of cleaved caspase-3 and Bcl2-associated X protein (Bax) proteins in rat myocardial tissue, while the level of B-cell lymphoma-2 (Bcl-2) protein was significantly reduced. DAPA pre-treatment markedly reduced the expression of cleaved caspase-3 and Bax, while simultaneously increasing the level of Bcl-2 (Fig. 5B–E). However, co-treatment with EX-527 remarkably reversed the inhibitory effect of DAPA on apoptosis in rat cardiomyocytes. Overall, the results suggest that the positive effects of DAPA on CME are correlated with the inhibition of cardiomyocyte apoptosis.

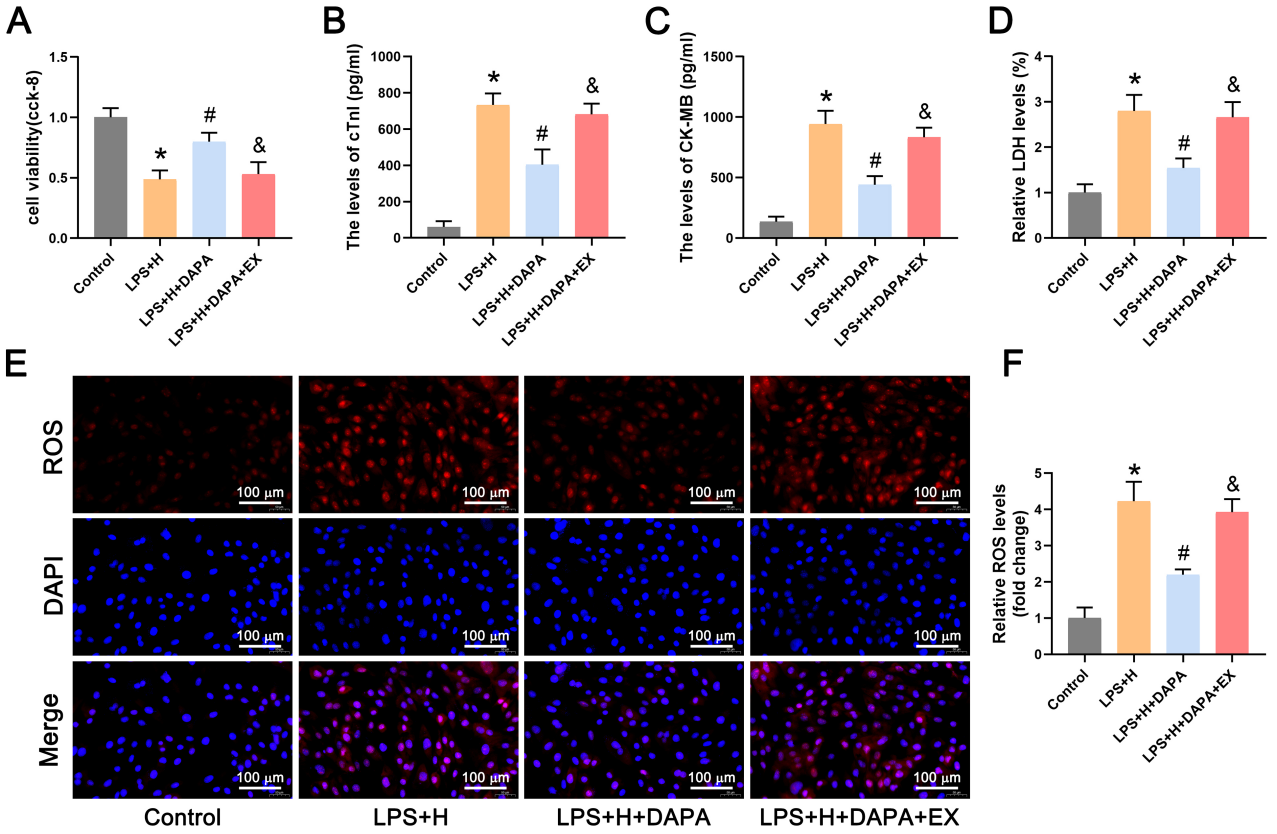

Fig. 3. DAPA attenuates H9C2 cardiomyocyte injury induced by the combination of LPS and hypoxia. (A) A CCK-8 assay was used to evaluate cell viability (n = 5). (B–D) The levels of cTnI, CK-MB, and LDH in the cell culture supernatant of each group (n = 5). (E,F) ROS levels were determined through DHE fluorescence probing (×200; scale bar = 100 μm) (n = 5). $^{*}p < 0.05$ vs. the Control group; $^{\#}p < 0.05$ vs. the LPS+H group; $^{\&}p < 0.05$ vs. the LPS+H+DAPA group. Abbreviations: LPS+H, lipopolysaccharide + hypoxia; DHE, dihydroethidium.

3.6 DAPA Attenuates H9C2 Cardiomyocyte Apoptosis Induced by LPS Combined with Hypoxia

Apoptosis assessed using TUNEL staining in an *in vitro* study. Relative to controls, the staining revealed a significantly elevated proportion of TUNEL-positive nuclei in the LPS+H group which was markedly reduced following DAPA pre-treatment (Fig. 6A). The levels of apoptosis-related protein expression were analyzed using IF staining and WB. The cleaved caspase-3 and Bax protein contents of H9C2 cardiomyocytes of the LPS+H group increased considerably in comparison to the control group, whereas Bcl-2 protein expression levels were markedly reduced. DAPA pretreatment substantially decreased the levels of cleaved caspase-3 and Bax, while simultaneously enhancing the level of Bcl-2 (Fig. 6B–E). In contrast, the inhibiting impact of DAPA on apoptosis in H9C2 cells was substantially reversed by co-treatment with EX-527. As a result, these data offer evidence of DAPA's involvement in the reduction of apoptosis in cardiomyocytes.

3.7 DAPA Regulates CME-Induced Heart Damage via the SIRT1/ NF-κB Signaling Pathway

The levels of SIRT1 in heart tissue and the levels of NF-κB pathway-related biomarkers were detected using WB and immunofluorescence to investigate whether DAPA improves CME-induced myocardial damage is related to the SIRT1/NF-κB axis. In contrast to the sham group, the WB results demonstrated that the levels of Ace-p65 and P-p65 proteins, as well as total P65 protein expression were enhanced, whereas SIRT1 protein levels were substantially reduced in the CME group. However, relative to the CME group, DAPA pre-treatment increased SIRT1 protein expression, while decreasing the levels of Ace-p65 and P-p65 proteins, as well as total p65 protein expression (Fig. 7A). The impacts of DAPA on the expression of the SIRT1/NF-κB axis were reversed after co-treatment with EX-527. The IF results of SIRT1 in myocardial tissue were consistent with the WB results (Fig. 7B). Simultaneously, the WB results of H9C2 cardiomyocytes in vitro are consistent with the results of animal experiments. DAPA treatment increased SIRT1 protein expression, while decreasing the levels of Ace-p65 and P-p65 proteins, as well as total p65 protein expression (Fig. 7C). The effects of DAPA were reversed after co-treatment with EX-527. The IF findings of SIRT1 in H9C2 cardiomyocytes were also consistent with the WB results (Fig. 7D). Overall, the combined results of both experimental studies indicate that DAPA reduces CME-induced myocarditis and apoptosis by modulat-

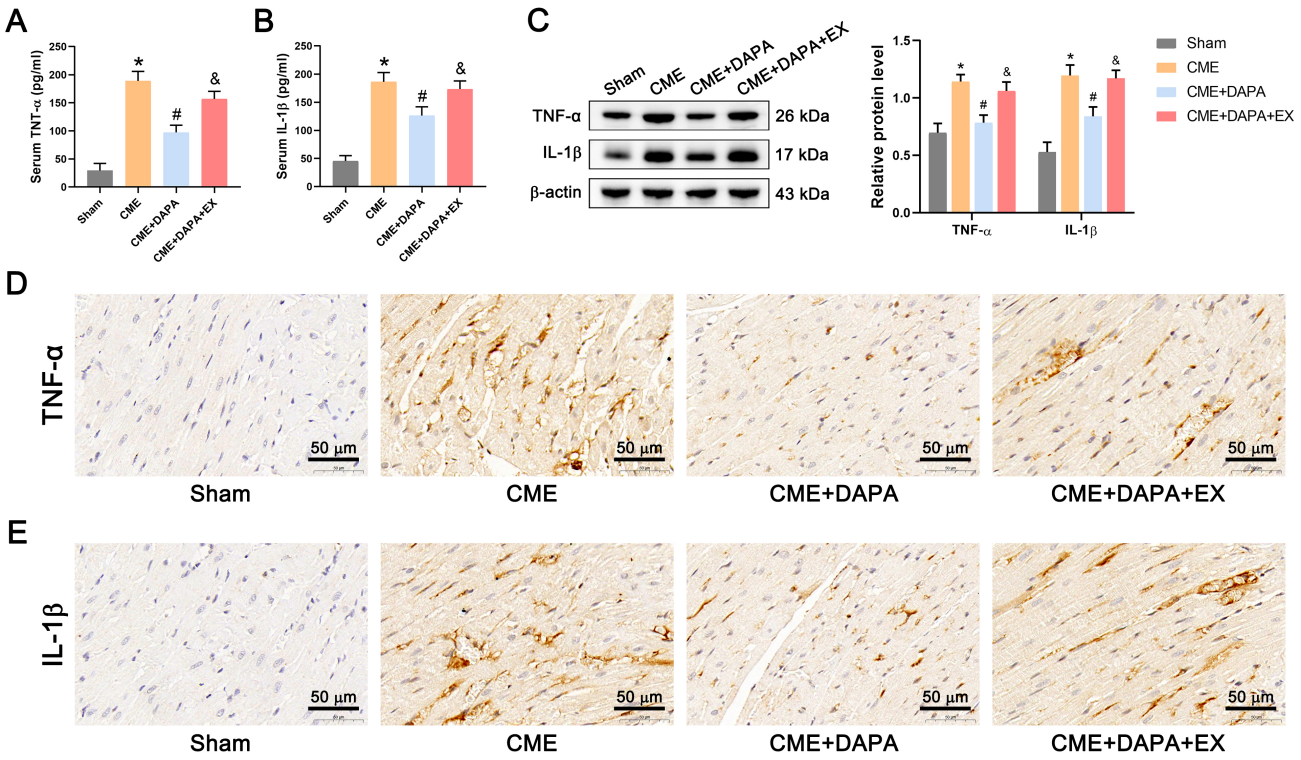

Fig. 4. DAPA attenuates CME-induced myocardial inflammatory injury. (A,B) Measurement of TNF-α and IL-1β in serum samples (n = 10). (C) TNF-α and IL-1β protein expression in the myocardia (n = 5). (D,E) Representative immunohistochemical images of TNF-α and IL-1β (×400; scale bar = 50 μm). *$p < 0.05$ vs. the Sham group; $^{\#}p < 0.05$ vs. the CME group; $^{\&}p < 0.05$ vs. the CME + DAPA group. Abbreviations: TNF-α, tumor necrosis factor-α; IL-1β, interleukin-1β.

ing the SIRT1/NF-κB axis and decreasing p65 acetylation and phosphorylation levels (Fig. 8).

4. Discussion

This study has revealed novel discoveries. The findings indicate that DAPA effectively reduces myocarditis and apoptosis, thereby reducing CME-caused myocardial damage, as evidenced by the development of a rat CME model and an in vitro model of LPS + hypoxia-induced cardiomyocytes. To the best of the current understanding, this is the first investigation of the role of DAPA on myocarditis and cell apoptosis in this specific CVD animal model. Further studies, utilizing EX-527, have revealed that DAPA attenuates myocarditis and apoptosis after CME by modulating the SIRT1/NF-κB axis. This, in turn, leads to the amelioration of CME-induced cardiac dysfunction and a reduction in myocardial damage. Thus, DAPA showed promising therapeutic potential for CME-induced heart damage.

The extent of cardiac function impairment induced by CME is not directly proportional to the reduction in coronary blood flow [28]. Hence, with the occurrence of CME-induced myocardial damage, there must be additional factors beyond the direct damage resulting from reduced blood flow. Previous research has shown that cardiomyocyte apoptosis and inflammation are significant factors in the occurrence of myocardial damage following CME, especially for the typical myocardial tissue near microinfarct regions [9,29]. The suppression of cardiac apoptosis and inflammation has been shown to significantly improve cardiac dysfunction resulting from CME. This study demonstrated that the heart function of rats in the CME model was considerably impaired relative to that of the sham group, and the degree of cardiomyocyte apoptosis and inflammation was worse in the CME model. All these results are consistent with previous research.

A novel class of hypoglycemic agents, SGLT-2i, has demonstrated remarkable cardioprotective properties, including the prevention of atherosclerotic events and the preservation of renal function [30]. Previously, it was considered that the cardioprotective effect of SGLT-2i was a result of their diuretic and antihypertensive impacts, which decrease ventricular burden [31]. According to a study, DAPA reduces cardiac damage by blocking electrical remodeling and cardiomyocyte apoptosis via the phosphatidylinositol 3-kinase (PI3K)/protein kinase B (AKT) signaling cascade [32]. Another study demonstrates that DAPA regulates AKT-mediated OS, cardiac renovation, and inflammation, thereby reducing doxorubicin-induced myocardial damage [33]. These results indicate that DAPA's cardioprotective effects may involve additional mechanisms. The current results suggested that the stimulation of myocardial injury by CME and LPS + hypoxia resulted in substantial myocarditis and cardiomyocyte apoptosis. However, the aberrant alterations were

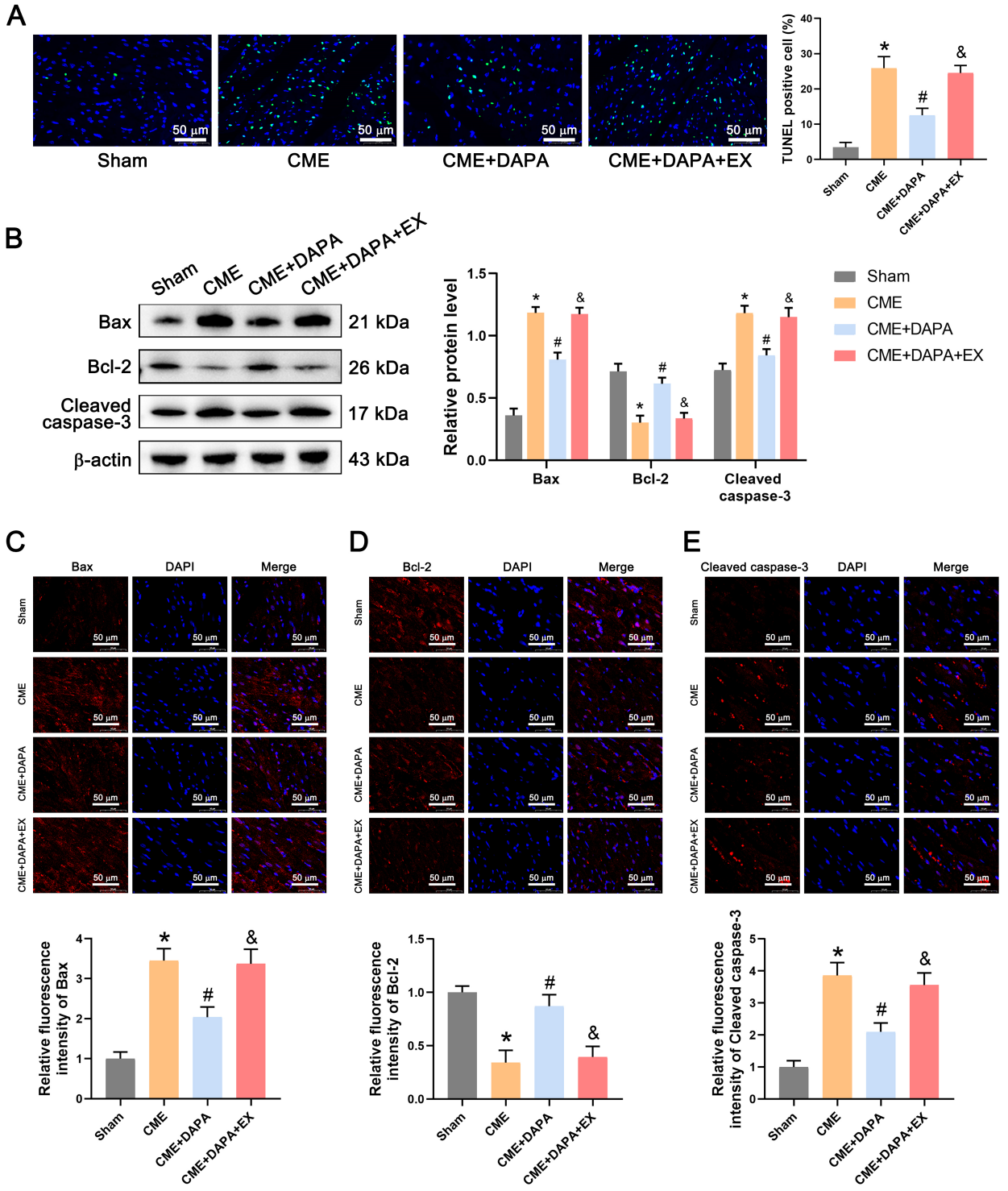

Fig. 5. DAPA attenuates cardiomyocyte apoptosis induced by CME. (A) Representative TUNEL staining images of myocardial tissue in each group and quantitative analysis of TUNEL-positive cells (×400; scale bar = 50 μm) (n = 10). (B) Protein expression levels of cleaved caspase-3, Bax, and Bcl-2 in the myocardium (n = 5). (C–E) Representative fluorescence images and relative fluorescence intensity of cleaved caspase-3, Bax, and Bcl-2 in the myocardium in each group (×400; scale bar = 50 μm) (n = 10). *$p < 0.05$ vs. the Sham group; $^{\#}p < 0.05$ vs. the CME group; $^{\&}p < 0.05$ vs. the CME + DAPA group. Abbreviations: Bax, BCL2-associated X protein; Bcl-2, B-cell lymphoma-2.

successfully repaired by the DAPA pretreatment. Therefore, the direct cardiac mechanism of DAPA may clarify the explanation of these findings. Based on the experimental outcomes of this study, the direct effect of DAPA occurs by reducing mitochondrial dysfunction, ROS production, cardiac inflammation and apoptosis, and the ability to activate

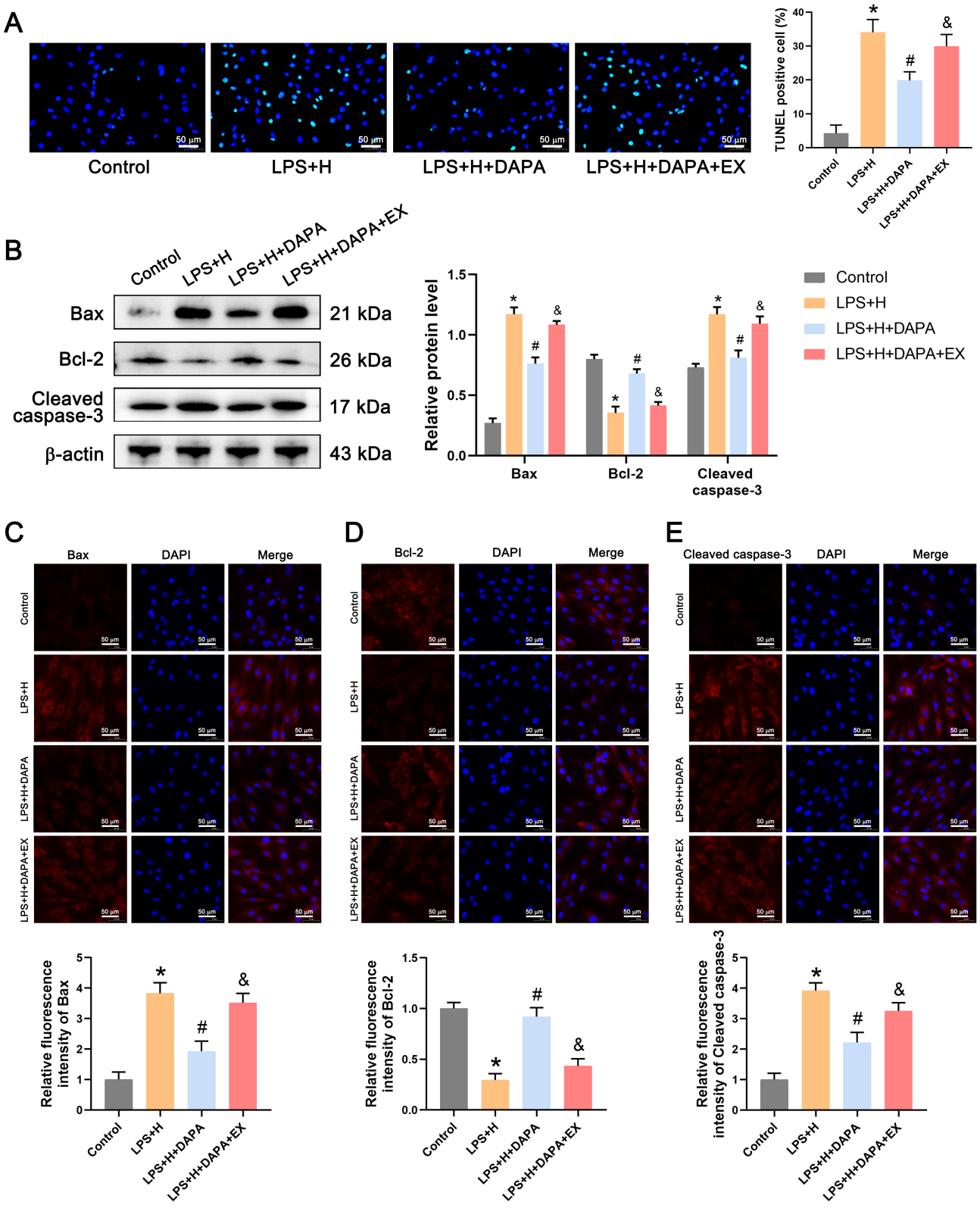

Fig. 6. DAPA attenuates H9C2 cardiomyocyte apoptosis induced by the combination of LPS and hypoxia. (A) Representative images of TUNEL-stained cells and quantitative assessment of TUNEL-positive cells in each group (×400; scale bar = 50 μm) (n = 5). (B) Protein expression levels of cleaved caspase-3, Bax, and Bcl-2 in H9C2 cardiomyocytes (n = 5). (C–E) Representative fluorescence images and relative fluorescence intensity of cleaved caspase-3, Bax, and Bcl-2 in H9C2 cardiomyocytes in each group (×400; scale bar = 50 μm) (n = 5). *$p < 0.05$ vs. the Control group; $^{\#}p < 0.05$ vs. the LPS+H group; $^{\&}p < 0.05$ vs. the LPS+H+DAPA group.

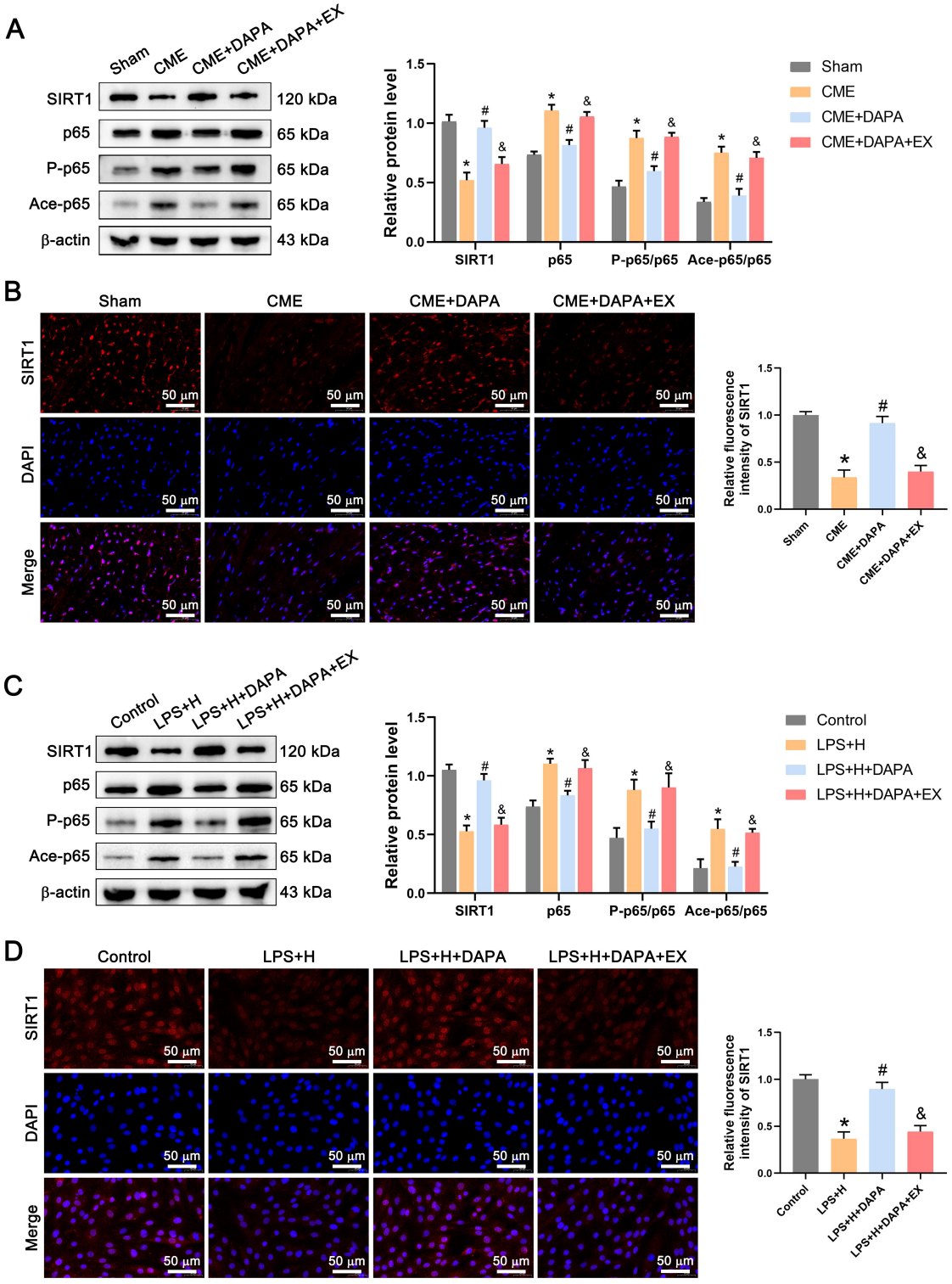

Fig. 7. DAPA regulates CME-induced myocardial injury through the SIRT1/ NF-κB signaling pathway. (A) Myocardial protein levels of NF-κB p65, Ace-p65, P-p65, and SIRT1 (n = 5). (B) Representative fluorescence images and comparative SIRT1 fluorescence levels in the myocardium of each group (×400; scale bar = 50 μm) (n = 10). (C) H9C2 cardiomyocyte protein expression of NF-κB p65, Ace-p65, P-p65, and SIRT1 (n = 5). (D) Representative fluorescence images and SIRT1 fluorescence quantification in H9C2 cardiomyocytes of each group (×400; scale bar = 50 μm) (n = 5). *$p < 0.05$ vs. the Sham group; $^{\#}p < 0.05$ vs. the CME group; $^{\&}p < 0.05$ vs. the CME + DAPA group. Abbreviations: SIRT1, sirtuin 1.

SIRT1.

SIRT1 was the first SIRT protein identified in mam-

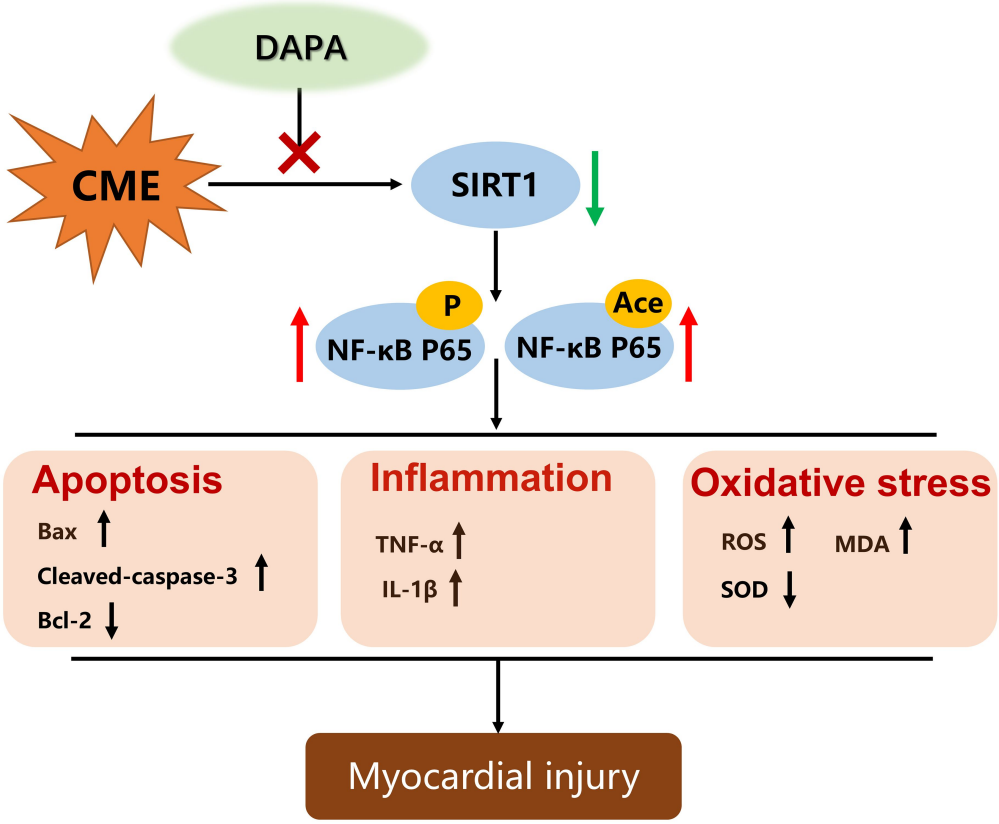

Fig. 8. Schematic figure of the mechanism by which dapagliflozin attenuates myocardial inflammation and apoptosis after CME via regulation of the SIRT1/NF-κB signaling pathway.

mals, and it is widely recognized for its involvement in improving life expectancy [34]. SIRT1 has a strong association with CVDs. For example, Hesperetin regulates the SIRT1/Nrf2 axis to prevent myocardial ischemia by inhibiting OS, inflammation, and apoptosis [35]. NF-κB is a nuclear transcription factor that is essential for the regulation of cellular immune and inflammatory responses. SIRT1 blocks inflammatory reactions triggered by the NF-κB pathway by deacetylating the p65 subunit of the NF-κB complex [36]. Ginsenoside Rg3 reduces angiotensin II-induced cardiac hypertrophy by blocking the nod-like receptor protein 3 (NLRP3)-mediated inflammation and OS through regulation of the SIRT1/NF-κB pathway [37]. During both normal and abnormal physiological states, NF-κB undergoes several different post-translational changes, including acetylation and phosphorylation [38]. Acetylation, combined with phosphorylation, has a significant impact on the regulation of NF-κB's nuclear activity [39]. Studies showed that the induction of NF-κB can cause inflammation and apoptosis in the tissue of the heart. Prolonged activation of p65 worsens cardiac damage by stimulating inflammation, fibrosis, and apoptosis [40,41]. In contrast, inhibiting the triggering of NF-κB activation can alleviate pro-inflammatory cytokines and cell apoptosis, further improving cardiac dysfunction [42,43]. The current findings suggest that the expression of SIRT1 is reduced in a CME model and an in vitro model of LPS + hypoxia-induced cardiomyocytes, while NF-κB activity is elevated, including increased levels of acetylation and phosphorylation. Further, pre-treatment with DAPA can reverse this situation, including activation of SIRT1 in the rat heart, improvement of cardiac function in CME rats, and reduction of NF-κB p65 acetylation and phosphorylation levels. Further study has demonstrated that the protective role of DAPA on cardiomyocytes was inhibited when SIRT1 inhibitor EX527 was administered, and NF-κB p65 acetylation and phosphorylation levels were equally elevated. The results demonstrate that SIRT1 is a critical factor in cardiomyocyte apoptosis and inflammation following CME. The association is attributed to the suppression of NF-κB activation.

There are also specific limitations associated with this study. First, the CME model in this research employed polyethylene microspheres to induce physical blockage, which may not fully replicate the physiological alterations observed in CME as a result of atheromatous plaque rupture in the actual physiological state of the body. Second, H9C2 cardiomyocytes were used instead of primary cardiomyocytes. It is crucial to acknowledge that H9C2 cells may not completely reflect all the attributes of primary cardiac cells, and any potential disparities should be duly con-

sidered. Third, further studies are demanded to evaluate if additional signaling cascades or mechanisms are implicated in CME-induced heart damage.

5. Conclusions

In summary, DAPA inhibits myocardial inflammation and apoptosis through regulation of the SIRT1/NF-κB signaling pathway, thereby protecting against injury to the myocardium induced by CME. This study elucidates the possible mechanistic role of the cardioprotective impact of DAPA and establishes a groundwork for the use of DAPA in preventing and treating CME-induced heart damage.

Availability of Data and Materials

The data used to support the findings of this study are available from the corresponding author on reasonable request.

Author Contributions

TL and LL conceived and designed the study. TL, CL, and ZY performed the experiments. TL and CL analyzed the data. TL drafted the manuscript, TL, CL, and LL revised it critically for important intellectual content. All authors contributed to editorial changes in the manuscript. All authors read and approved the final manuscript. All authors have participated sufficiently in the work and agreed to be accountable for all aspects of the work.

Ethics Approval and Consent to Participate

Protocols involving animals were approved by the Animal Care & Welfare Committee of Guangxi Medical University (Approval No. 202301010). All animal-related experiments, conducted in accordance with the established standards and procedures of the National Institutes of Health.

Acknowledgment

Not applicable.

Funding

This work was supported by the National Natural Science Foundation of China (No. 82170349).

Conflict of Interest

The authors declare no conflict of interest.

References

[1] Heusch G, Skyschally A, Kleinbongard P. Coronary microembolization and microvascular dysfunction. International Journal of Cardiology. 2018; 258: 17–23. https://doi.org/10.1016/j.ijcard.2018.02.010.

[2] Heusch G, Kleinbongard P, Böse D, Levkau B, Haude M, Schulz R, *et al*. Coronary microembolization: from bedside to bench and back to bedside. Circulation. 2009; 120: 1822–1836. https://doi.org/10.1161/CIRCULATIONAHA.109.888784.

[3] Kleinbongard P, Heusch G. A fresh look at coronary microembolization. Nature Reviews. Cardiology. 2022; 19: 265–280. https://doi.org/10.1038/s41569-021-00632-2.

[4] Ndrepepa G, Tiroch K, Fusaro M, Keta D, Seyfarth M, Byrne RA, *et al*. 5-year prognostic value of no-reflow phenomenon after percutaneous coronary intervention in patients with acute myocardial infarction. Journal of the American College of Cardiology. 2010; 55: 2383–2389. https://doi.org/10.1016/j.jacc.2009.12.054.

[5] Milasinovic D, Nedeljkovic O, Maksimovic R, Sobic-Saranovic D, Dukic D, Zobenica V, *et al*. Coronary Microcirculation: The Next Frontier in the Management of STEMI. Journal of Clinical Medicine. 2023; 12: 1602. https://doi.org/10.3390/jcm12041602.

[6] Scarpone M, Cenko E, Manfrini O. Coronary No-Reflow Phenomenon in Clinical Practice. Current Pharmaceutical Design. 2018; 24: 2927–2933. https://doi.org/10.2174/1381612824666180702112536.

[7] Jaffe R, Charron T, Puley G, Dick A, Strauss BH. Microvascular obstruction and the no-reflow phenomenon after percutaneous coronary intervention. Circulation. 2008; 117: 3152–3156. https://doi.org/10.1161/CIRCULATIONAHA.107.742312.

[8] Li T, Chen Z, Zhou Y, Li H, Xie J, Li L. Resveratrol Pretreatment Inhibits Myocardial Apoptosis in Rats Following Coronary Microembolization via Inducing the PI3K/Akt/GSK-3β Signaling Cascade. Drug Design, Development and Therapy. 2021; 15: 3821–3834. https://doi.org/10.2147/DDDT.S323555.

[9] Chen ZQ, Zhou Y, Chen F, Huang JW, Zheng J, Li HL, *et al*. Breviscapine Pretreatment Inhibits Myocardial Inflammation and Apoptosis in Rats After Coronary Microembolization by Activating the PI3K/Akt/GSK-3β Signaling Pathway. Drug Design, Development and Therapy. 2021; 15: 843–855. https://doi.org/10.2147/DDDT.S293382.

[10] Yang Y, Liu Y, Wang Y, Chao Y, Zhang J, Jia Y, *et al*. Regulation of SIRT1 and Its Roles in Inflammation. Frontiers in Immunology. 2022; 13: 831168. https://doi.org/10.3389/fimmu.2022.831168.

[11] Rada P, Pardo V, Mobasher MA, García-Martínez I, Ruiz L, González-Rodríguez Á, *et al*. SIRT1 Controls Acetaminophen Hepatotoxicity by Modulating Inflammation and Oxidative Stress. Antioxidants & Redox Signaling. 2018; 28: 1187–1208. https://doi.org/10.1089/ars.2017.7373.

[12] Xu C, Wang L, Fozouni P, Evjen G, Chandra V, Jiang J, *et al*. SIRT1 is downregulated by autophagy in senescence and ageing. Nature Cell Biology. 2020; 22: 1170–1179. https://doi.org/10.1038/s41556-020-00579-5.

[13] He F, Li Q, Sheng B, Yang H, Jiang W. SIRT1 Inhibits Apoptosis by Promoting Autophagic Flux in Human Nucleus Pulposus Cells in the Key Stage of Degeneration via ERK Signal Pathway. BioMed Research International. 2021; 2021: 8818713. https://doi.org/10.1155/2021/8818713.

[14] Tu C, Wan B, Zeng Y. Ginsenoside Rg3 alleviates inflammation in a rat model of myocardial infarction via the SIRT1/NF-κB pathway. Experimental and Therapeutic Medicine. 2020; 20: 238. https://doi.org/10.3892/etm.2020.9368.

[15] Lee WC, Lin YS, Chen MJ, Ho WC, Chen HC, Chang TH, *et al*. Downregulation of SIRT1 and GADD45G genes and left atrial fibrosis induced by right ventricular dependent pacing in a complete atrioventricular block pig model. Biomolecules & Biomedicine. 2024; 24: 360–373. https://doi.org/10.17305/bb.2023.9636.

[16] Mao Q, Liang X, Wu Y, Lu Y. Resveratrol Attenuates Cardiomyocyte Apoptosis in Rats Induced by Coronary Microembolization Through SIRT1-Mediated Deacetylation of p53. Journal of Cardiovascular Pharmacology and Therapeutics. 2019; 24: 551–558. https://doi.org/10.1177/1074248419845916.

[17] Vrhovac I, Balen Eror D, Klessen D, Burger C, Breljak D, Kraus O, *et al*. Localizations of Na(+)-D-glucose cotransporters SGLT1 and SGLT2 in human kidney and of SGLT1 in human

small intestine, liver, lung, and heart. Pflugers Archiv: European Journal of Physiology. 2015; 467: 1881–1898. https://doi.org/10.1007/s00424-014-1619-7.

[18] Li Z, Jia J, Hao H, Qiao S, Zhang Q, Zhang X, *et al*. Anti-Diabetic Drugs Inhibit Bulimia Induced Obesity. Frontiers in Bioscience (Landmark Edition). 2023, 28: 97. https://doi.org/10.31083/j.fbl2805097.

[19] Cowie MR, Fisher M. SGLT2 inhibitors: mechanisms of cardiovascular benefit beyond glycaemic control. Nature Reviews. Cardiology. 2020; 17: 761–772. https://doi.org/10.1038/s41569-020-0406-8.

[20] Kaplinsky E. DAPA-HF trial: dapagliflozin evolves from a glucose-lowering agent to a therapy for heart failure. Drugs in Context. 2020; 9: 2019-11-3. https://doi.org/10.7573/dic.2019-11-3.

[21] Packer M. Cardioprotective Effects of Sirtuin-1 and Its Downstream Effectors: Potential Role in Mediating the Heart Failure Benefits of SGLT2 (Sodium-Glucose Cotransporter 2) Inhibitors. Circulation. Heart Failure. 2020; 13: e007197. https://doi.org/10.1161/CIRCHEARTFAILURE.120.007197.

[22] Faridvand Y, Kazemzadeh H, Vahedian V, Mirzajanzadeh P, Nejabati HR, Safaie N, *et al*. Dapagliflozin attenuates high glucose-induced endothelial cell apoptosis and inflammation through AMPK/SIRT1 activation. Clinical and Experimental Pharmacology & Physiology. 2022; 49: 643–651. https://doi.org/10.1111/1440-1681.13638.

[23] Ren FF, Xie ZY, Jiang YN, Guan X, Chen QY, Lai TF, *et al*. Dapagliflozin attenuates pressure overload-induced myocardial remodeling in mice via activating SIRT1 and inhibiting endoplasmic reticulum stress. Acta Pharmacologica Sinica. 2022; 43: 1721–1732. https://doi.org/10.1038/s41401-021-00805-2.

[24] Tanajak P, Sa-Nguanmoo P, Sivasinprasasn S, Thummasorn S, Siri-Angkul N, Chattipakorn SC, *et al*. Cardioprotection of dapagliflozin and vildagliptin in rats with cardiac ischemia-reperfusion injury. The Journal of Endocrinology. 2018; 236: 69–84. https://doi.org/10.1530/JOE-17-0457.

[25] Lahnwong C, Palee S, Apaijai N, Sriwichaiin S, Kerdphoo S, Jaiwongkam T, *et al*. Acute dapagliflozin administration exerts cardioprotective effects in rats with cardiac ischemia/reperfusion injury. Cardiovascular Diabetology. 2020; 19: 91. https://doi.org/10.1186/s12933-020-01066-9.

[26] Fan ZG, Xu Y, Chen X, Ji MY, Ma GS. Appropriate Dose of Dapagliflozin Improves Cardiac Outcomes by Normalizing Mitochondrial Fission and Reducing Cardiomyocyte Apoptosis After Acute Myocardial Infarction. Drug Design, Development and Therapy. 2022; 16: 2017–2030. https://doi.org/10.2147/DDDT.S371506.

[27] Liu Y, Shu J, Liu T, Xie J, Li T, Li H, *et al*. Nicorandil protects against coronary microembolization-induced myocardial injury by suppressing cardiomyocyte pyroptosis via the AMPK/TXNIP/NLRP3 signaling pathway. European Journal of Pharmacology. 2022; 936: 175365. https://doi.org/10.1016/j.ejphar.2022.175365.

[28] Heusch G. The regional myocardial flow-function relationship: a framework for an understanding of acute ischemia, hibernation, stunning and coronary microembolization. 1980. Circulation Research. 2013; 112: 1535–1537. https://doi.org/10.1161/CIRCRESAHA.113.301446.

[29] Wang JY, Chen H, Su X, Zhou Y, Li L. Atorvastatin Pretreatment Inhibits Myocardial Inflammation and Apoptosis in Swine After Coronary Microembolization. Journal of Cardiovascular Pharmacology and Therapeutics. 2017; 22: 189–195. https://doi.org/10.1177/1074248416662348.

[30] Zelniker TA, Braunwald E. Mechanisms of Cardiorenal Effects of Sodium-Glucose Cotransporter 2 Inhibitors: JACC State-of-the-Art Review. Journal of the American College of Cardiology. 2020; 75: 422–434. https://doi.org/10.1016/j.jacc.2019.11.031.

[31] Joshi SS, Singh T, Newby DE, Singh J. Sodium-glucose co-transporter 2 inhibitor therapy: mechanisms of action in heart failure. Heart. 2021; 107: 1032–1038. https://doi.org/10.1136/heartjnl-2020-318060.

[32] Han X, Liu X, Zhao X, Wang X, Sun Y, Qu C, *et al*. Dapagliflozin ameliorates sepsis-induced heart injury by inhibiting cardiomyocyte apoptosis and electrical remodeling through the PI3K/Akt pathway. European Journal of Pharmacology. 2023; 955: 175930. https://doi.org/10.1016/j.ejphar.2023.175930.

[33] Hsieh PL, Chu PM, Cheng HC, Huang YT, Chou WC, Tsai KL, *et al*. Dapagliflozin Mitigates Doxorubicin-Caused Myocardium Damage by Regulating AKT-Mediated Oxidative Stress, Cardiac Remodeling, and Inflammation. International Journal of Molecular Sciences. 2022; 23: 10146. https://doi.org/10.3390/ijms231710146.

[34] Bonkowski MS, Sinclair DA. Slowing ageing by design: the rise of NAD^+ and sirtuin-activating compounds. Nature Reviews. Molecular Cell Biology. 2016; 17: 679–690. https://doi.org/10.1038/nrm.2016.93.

[35] Liu P, Li J, Liu M, Zhang M, Xue Y, Zhang Y, *et al*. Hesperetin modulates the Sirt1/Nrf2 signaling pathway in counteracting myocardial ischemia through suppression of oxidative stress, inflammation, and apoptosis. Biomedicine & Pharmacotherapy. 2021; 139: 111552. https://doi.org/10.1016/j.biopha.2021.111552.

[36] Liu P, Li Y, Wang W, Bai Y, Jia H, Yuan Z, *et al*. Role and mechanisms of the NF-κB signaling pathway in various developmental processes. Biomedicine & Pharmacotherapy. 2022; 153: 113513. https://doi.org/10.1016/j.biopha.2022.113513.

[37] Ren B, Feng J, Yang N, Guo Y, Chen C, Qin Q. Ginsenoside Rg3 attenuates angiotensin II-induced myocardial hypertrophy through repressing NLRP3 inflammasome and oxidative stress via modulating SIRT1/NF-κB pathway. International Immunopharmacology. 2021; 98: 107841. https://doi.org/10.1016/j.intimp.2021.107841.

[38] Chen LF, Williams SA, Mu Y, Nakano H, Duerr JM, Buckbinder L, *et al*. NF-kappaB RelA phosphorylation regulates RelA acetylation. Molecular and Cellular Biology. 2005; 25: 7966–7975. https://doi.org/10.1128/MCB.25.18.7966-7975.2005.

[39] Chen LF, Mu Y, Greene WC. Acetylation of RelA at discrete sites regulates distinct nuclear functions of NF-kappaB. The EMBO Journal. 2002; 21: 6539–6548. https://doi.org/10.1093/emboj/cdf660.

[40] Hamid T, Guo SZ, Kingery JR, Xiang X, Dawn B, Prabhu SD. Cardiomyocyte NF-κB p65 promotes adverse remodelling, apoptosis, and endoplasmic reticulum stress in heart failure. Cardiovascular Research. 2011; 89: 129–138. https://doi.org/10.1093/cvr/cvq274.

[41] Xue Y, Zhang J, Ke J, Zeng L, Cheng K, Han X, *et al*. LncGBP9 knockdown alleviates myocardial inflammation and apoptosis in mice with acute viral myocarditis via suppressing NF-κB signaling pathway. Inflammation Research. 2022; 71: 1559–1576. https://doi.org/10.1007/s00011-022-01644-5.

[42] Jiang F, Xu XR, Li WM, Xia K, Wang LF, Yang XC. Monotropein alleviates H2O2 induced inflammation, oxidative stress and apoptosis via NF κB/AP 1 signaling. Molecular Medicine Reports. 2020; 22: 4828–4836. https://doi.org/10.3892/mmr.2020.11548.

[43] Meng YY, Liu Y, Hu ZF, Zhang Y, Ni J, Ma ZG, *et al*. Sanguinarine Attenuates Lipopolysaccharide-induced Inflammation and Apoptosis by Inhibiting the TLR4/NF-κB Pathway in H9c2 Cardiomyocytes. Current Medical Science. 2018; 38: 204–211. https://doi.org/10.1007/s11596-018-1867-4.